Adaptive flux-based nodeless variable finite element formulation with error estimation for thermal-structural analysis

S Traivivatana[1], S Phongthanapanich[2] and P Dechaumphai [3,4]
[1] Energy Research Institute, Chulalongkorn University, Bangkok 10330, Thailand
[2] Department of Mechanical Engineering Technology, College of Industrial Technology, King Mongkut's University of Technology North Bangkok, Bangkok 10800, Thailand
[3] Department of Mechanical Engineering, Chulalongkorn University, Bangkok 10330, Thailand

Abstract. A posteriori error estimation for the nodeless variable finite element method is presented. A nodeless variable finite element method using flux-based formulation is developed and combined with an adaptive meshing technique to analyze two-dimensional thermal-structural problems. The continuous flux and stresses are determined by using the flux-based formulation while the standard linear element interpolation functions are used to determine the discontinuous flux and stresses. To measure the global error, the L_2 norm error is selected to find the root-mean-square error over the entire domain. The finite element formulation and its detailed finite element matrices are presented. Accuracy of the estimated error is measured by the percentage relative error. An adaptive meshing technique, that can generate meshes corresponding to solution behaviors automatically, is implemented to further improve the solution accuracy. Several examples are presented to evaluate the performance and accuracy of the combined method.

1. Introduction

The finite element method has been widely used to analyze many engineering problems [1,2]. Both triangular and tetrahedral elements are frequently used due to the simplicity for constructing meshes for complex geometry problems but the solution accuracy is normally low. Since the thermal stresses are sensitive to the predicted thermal gradients, a more accurate thermal analysis is required to predict temperature distribution. The solution accuracy may be improved using the *h*-method of adaptation where the mesh is globally or locally refined or coarsened [3,4].

The objective of this paper is to develop a nodeless variable finite element method to improve the predicted solution of the two-dimensional Poisson's equation. The nodeless variable finite elements use the quadratic interpolation functions to express the solution distribution over the element without requiring additional actual nodes. In addition, the paper introduces and applies the flux-based formulation to derive the finite element matrices for such nodeless variable element.

An adaptive unstructured meshing technique [4,5] is implemented to improve the solution accuracy. The efficiency of the combined nodeless variable finite element method using flux-based formulation and the adaptive meshing technique is evaluated by several examples with exact solutions.

2. Nodeless variable finite element method

[1] To whom any correspondence should be addressed.

2.1. Governing equations and boundary conditions

The Poisson's equation for two-dimensional domain in *x-y* coordinate system as shown in figure 1 can be written in the conservation form as,

$$\frac{\partial \{E\}}{\partial x} + \frac{\partial \{F\}}{\partial y} = f(x,y) \tag{1}$$

where $f(x,y)$ denotes the source function. The flux vector components $\{E\}$ and $\{F\}$ contain the heat flux components for thermal analysis or the stress components for structural analysis given by,

$$\{E\} = -c\frac{\partial \{U\}}{\partial x} \quad \text{and} \quad \{F\} = -c\frac{\partial \{U\}}{\partial y} \tag{2}$$

where U is the primary variable and c is the material property that depends on types of problem. The Poisson's equation shown in equation (1) is to be solved together with appropriate boundary conditions that may consist of,

$$U_1(x,y) \quad \text{on } S_1 \tag{3a}$$

$$c\frac{\partial \{U\}}{\partial n} + d\left(\{U\} - U_\infty\right) = q \quad \text{on } S_2 \tag{3b}$$

where d and U_∞ are constants and q is the secondary variable.

2.2. Nodeless variable flux-based finite element formulation

The flux-based formulation [6] is implemented to derive the corresponding finite element equations for a nodeless variable element. For the triangular nodeless variable element, the distribution of the primary variable over the element is assumed in the form,

$$U(x,y) = \sum_{i=1}^{6} N_i(x,y)U_i = \lfloor N(x,y) \rfloor \{U\} \tag{4}$$

where $\lfloor N(x,y) \rfloor$ consists of the element interpolation functions, and $\{U\}$ is the vector of the unknown primary variables and the nodeless variables. The nodal primary variables are U_1 through U_3, while U_4 through U_6 are the nodeless variables. The element interpolation functions, N_1, N_2, N_3 are identical to the element interpolation functions L_1, L_2, L_3 used for the standard three-node triangular element. The nodeless variable interpolation functions implemented in this paper are,

$$N_4 = L_2L_3 \;;\; N_5 = L_1L_3 \;;\; N_6 = L_1L_2 \tag{5}$$

Each nodeless variable interpolation function varies quadratically along one edge and vanishes along the other edges. To derive the finite element matrices by means of the flux-based formulation, the method of weighted residuals is first applied to equation (1). The Gauss's theorem is then applied to the flux derivative terms to yield,

$$\int_\Omega \frac{\partial N_i}{\partial x}\{E\}\,d\Omega + \int_\Omega \frac{\partial N_i}{\partial y}\{F\}\,d\Omega = \int_S N_i\{E\}n_x\,d\Gamma + \int_S N_i\{F\}n_y\,d\Gamma - \int_\Omega N_i\,f(x,y)\,d\Omega \tag{6}$$

where Ω is the element domain and S is the element boundary.

In the flux-based formulation, the element flux distributions are computed from the actual nodal fluxes as,

$$\{E\} = \sum_{i=1}^{3} \overline{N}_i \{E_i\} = \lfloor \overline{N} \rfloor \{E^n\} \quad \text{and} \quad \{F\} = \sum_{i=1}^{3} \overline{N}_i \{F_i\} = \lfloor \overline{N} \rfloor \{F^n\} \tag{7}$$

where $\lfloor \overline{N} \rfloor$ are the standard linear element interpolation functions, i.e., $\lfloor L_1 \quad L_2 \quad L_3 \rfloor$. The $\{E^n\}$ and $\{F^n\}$ are the vectors of the actual nodal fluxes.

Determination of nodal fluxes depends on the types of problem considered. For structural analysis problem, the stress components σ_x, σ_y, τ_{xy} are related to the strain components by Hook's law. The compact form of equation (6) for structural analysis can be written as,

$$\int_{\Omega} [B]^T \{\sigma\} d\Omega = \int_{S} [N]^T \{T_S\} d\Gamma \tag{8}$$

where

$$[B] = \begin{bmatrix} \frac{\partial N_1}{\partial x} & 0 & \cdots & \frac{\partial N_6}{\partial x} & 0 \\ 0 & \frac{\partial N_1}{\partial y} & \cdots & 0 & \frac{\partial N_6}{\partial y} \\ \frac{\partial N_1}{\partial y} & \frac{\partial N_1}{\partial x} & \cdots & \frac{\partial N_6}{\partial y} & \frac{\partial N_6}{\partial x} \end{bmatrix}^T \quad \text{and} \quad [N] = \begin{bmatrix} N_1 & 0 & \cdots & N_6 & 0 \\ 0 & N_1 & \cdots & 0 & N_6 \end{bmatrix} \tag{9}$$

$$\{\sigma\} = \lfloor \sigma_x \quad \sigma_y \quad \tau_{xy} \rfloor^T$$

$$\{T_s\} = \lfloor T_{Sx} \quad T_{Sy} \rfloor^T$$

and $\{T_s\}$ is the boundary tractions vector which can be written as,

$$\{T_s\} = [\overline{N}]\{\overline{T}_s\} \tag{10}$$

where $[\overline{N}]$ and $\{\overline{T}_s\}$ are interpolation matrix and boundary tractions vector, respectively. The interpolation functions in equation (10) needed for integration along a typical element side *S* are,

$$N_1 = 1 - \frac{x}{L};\ N_2 = \frac{x}{L};\ N_3 = \frac{x}{L}\left(1 - \frac{x}{L}\right) \tag{11}$$

where *L* is the length of element edge and *x* is the local coordinate along the edge starting from node 1 as shown in figure 2. Appropriate boundary conditions of the structural analysis problem are then applied. Two types of the boundary conditions considered herein are the specified displacements and boundary tractions, as given by equations (3a) and (3b), respectively.

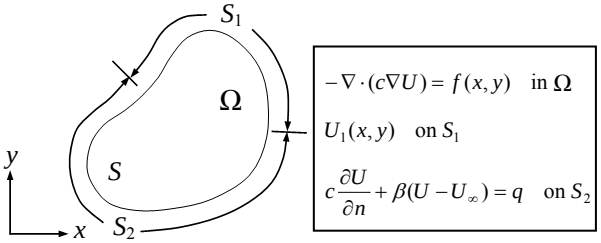

Figure 1. Two-dimensional domain and boundary conditions for Poisson's problem.

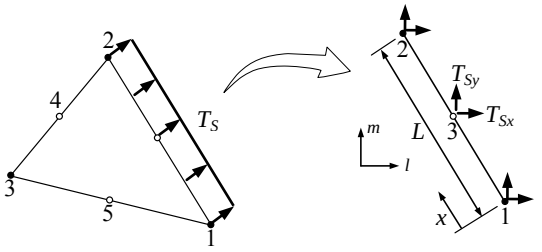

Figure 2. Discretization of boundary tractions into nodal quantities.

3. A posteriori error estimation

3.1. Flux-based formulation for nodal fluxes

Figure 3(a) shows the typical flux (heat flux or stress) distributions computed by using the conventional finite element formulation for standard triangles. Figure 3(b) shows the continuous flux distributions for the same triangular mesh by using the flux-based formulation.

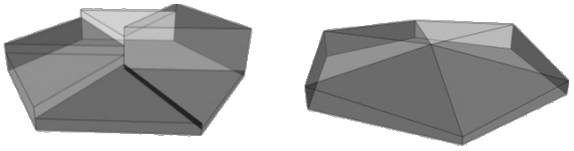

a) Discontinuous b) Continuous

Figure 3. Flux distributions.

Errors of fluxes are determined from the difference between the computed continuous and discontinuous fluxes. The errors of flux gradients are defined by

$$e_g = g^{FB} - g^{ST} \tag{12}$$

where g^{FB} are the flux-based element gradients and g^{ST} are the standard element gradients.

The method of weighted residuals is applied to equation (12) and substituting the element flux distributions from equation (7) to yield,

$$[M]\{\overline{g}^{FB}\} = [G]\{U\} \tag{13}$$

where $[M]$ is the mass matrix and $\{\overline{g}^{FB}\}$ is the vector of the flux-based nodal fluxes.

3.2. Error estimator

To measure the global error, the L_2 norm error is selected to find the root-mean-square error over the entire domain [7]. From equation (12), the square of the L_2 norm error for the gradients is

$$\left\| e_g^{FE} \right\|_{L_2}^2 = \int_{\Omega} (g^{FB} - g^{ST})^2 \, d\Omega \tag{14}$$

By applying the same concept onto the errors of gradients, the finite element equations for the finite element error square are,

$$\left\| e_g^{FE} \right\|_{L_2}^2 = \left\lfloor \overline{g}^{FB} \right\rfloor [M] \left[\overline{g}^{FB} \right] + \left\lfloor \overline{g}^{FB} \right\rfloor [G]\{U\} + \lfloor U \rfloor [K]\{U\} \tag{15}$$

The finite element global error for gradients is computed from

$$\left\| e_g^{FE} \right\|_g = \left[\sum_{element} \left\| e_g^{FE} \right\|_{L_2}^2 \Big/ A_d \right]^{1/2} \tag{16}$$

where A_d is the total domain area. The square of exact L_2 norm error for gradients is

$$\left\| e_g^{FB} \right\|_{L_2}^2 = \int_{\Omega} (g^{EX} - g^{FB})^2 \, d\Omega \quad \text{and} \quad \left\| e_g^{ST} \right\|_{L_2}^2 = \int_{\Omega} (g^{EX} - g^{ST})^2 \, d\Omega \tag{17}$$

where g^{EX} are exact element gradients, $\left\| e_g^{FB} \right\|_{L_2}^2$ and $\left\| e_g^{ST} \right\|_{L_2}^2$ are the square of error for flux-based element and standard element, respectively. The exact global error for both flux-based element and standard element are applied with the same procedure. From the concept of measuring discretization error in the elastic problem, the Z^2-error estimate [8], the percentage relative error is defined by,

$$\eta = \frac{\|\mathbf{e}\|_{L_2}}{\|\mathbf{u}\|_{L_2}} \times 100 \tag{18}$$

where $\|\mathbf{e}\|_{L_2}$ is the error in the L_2 norm and $\|\mathbf{u}\|_{L_2}$ is L_2 norm of the solution. The mesh adaptation is terminated when the value of η is less than 5% which is reasonable for engineering applications [9,10].

4. Numerical examples

To evaluate the performance and accuracy of the combined adaptive nodeless variable finite element method together with the flux-based formulation and the proposed error estimation method, two example problems are studied and presented. These problems are: (1) a square domain with source function and (2) an L-shaped plate under uniform loading.

4.1. Square domain with source function

A unit square domain with the specified boundary conditions is shown in figure 4. The specified source function over the plate [11] is given by,

$$f(x,y) = -14x(1-x)(1-2y) - 4y(1-y)(1-2x) + 2(1+2x+7y)\left[x(1-x) + y(1-y)\right] \tag{19}$$

The exact solution for the primary variable distribution is,

$$U(x,y) = x(1-x)\, y(1-y)(1+2x+7y) \tag{20}$$

Figure 5 shows the three structure finite element mesh models with 32, 128 and 512 nodeless variable finite elements, respectively. The first T3NL–M1, the second T3NL–M2 and the third

T3NL–M3 meshes consist of 25, 81 and 289 nodes, respectively. The figure also shows the predicted solution contours obtained from these mesh models.

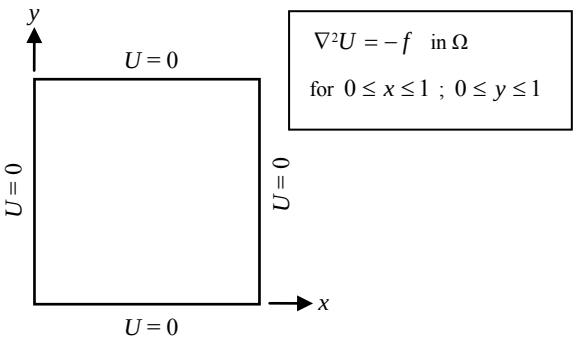

Figure 4. Problem statement of a unit square domain with specified source function.

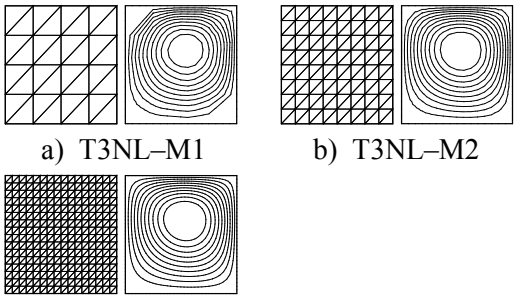

Figure 5. Three structured mesh models and their solution contours.

The comparisons between the exact and three nodeless variable flux-based finite element solutions along the edge x = 0.5 are shown in figure 6. The L_2 norm and percentage relative errors of the exact global error using the flux-based and standard elements together with the approximate global error are presented in Table 1. The table shows that the computed global errors for the three finite element mesh models are in the same trend as the exact errors. These global errors can be used for measuring the solution accuracy obtained from the finite element mesh models with different discretization.

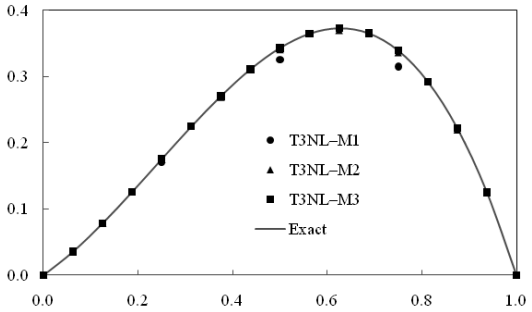

Figure 6. Comparison between the exact and three finite element solutions along the edge x = 0.5.

Table 1. Quantitative comparisons of global errors for a unit square domain with specified source function.

Element	$\left\| e_g^{FB} \right\|_g$, (η_{FB})	$\left\| e_g^{ST} \right\|_g$, (η_{ST})	$\left\| e_g^{FE} \right\|_g$, (η_{FE})
T3NL–M1	0.210 (19.98%)	0.283 (25.20%)	0.190 (19.22%)
T3NL–M2	0.065 (6.96%)	0.089 (9.29%)	0.061 (6.52%)
T3NL–M3	0.018 (1.99%)	0.025 (2.72%)	0.017 (1.88%)

4.2. L-shaped plate under uniform loading

This test case is a L-shaped domain [8] subjected to a tensile load of $\sigma = 1$ as shown in figure 7. The plane stress condition is assumed with the Poisson's ratio of 0.3 and Young's modulus E = 100,000.

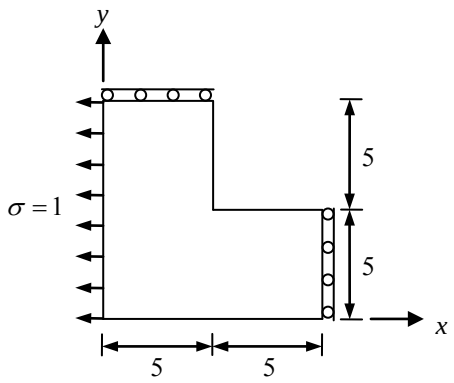

Figure 7. Problem statement of an L-shaped plate under uniform loading.

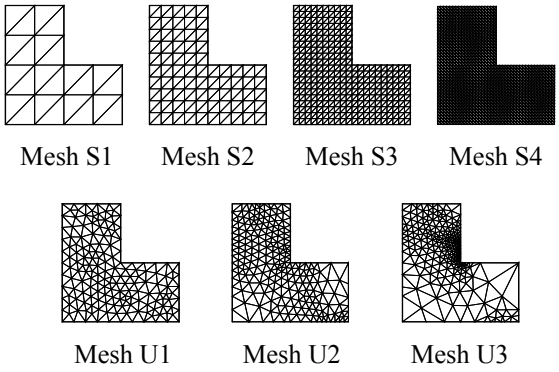

Figure 8. Meshes used in analysis of L-shaped plate under uniform loading.

Figure 8 shows the four uniform meshes (S1 to S4), an initial unstructured mesh (U1) and two adaptive meshes (U2 and U3) used in the analysis. The number of nodes in different meshes and the computed percentage errors of their solutions are tabulated in Table 2. The table also highlights performance of the adaptive meshing technique that the number of nodes are almost constant (228 and 257 nodes in mesh U2 and U3, respectively) during the adaptive process, whereas the final uniform mesh contains five times greater of the number of nodes (1,281 nodes in mesh S4) at the same error level. The comparison for the solution convergence rates between the uniform refinement meshes and the adaptive meshes are presented in figure 9 where *N* denotes the number of nodes. The solution convergence rates of the uniformly refine meshes is 0.36 as compared to 2.59 for the adaptive meshes. The convergence rates of the uniform refinement meshes are relatively low due to the solution singularity at the center corner.

Table 2. Quantitative comparisons of global errors for analysis of L-shaped plate under uniform loading

Element	Number of nodes	η_{FE}
Mesh S1	21	12.08%
Mesh S2	96	6.35%
Mesh S3	341	4.07%
Mesh S4	1,281	2.67%
Mesh U1	166	6.21%
Mesh U2	228	3.53%
Mesh U3	257	2.35%

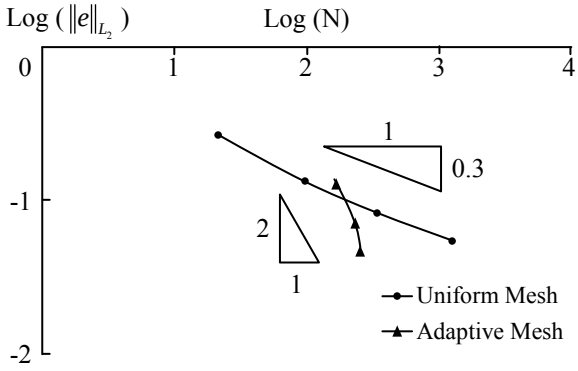

Figure 9. Comparison of solution convergences between the uniform refinement and adaptive meshes.

5. Conclusions

The nodeless variable finite element method using flux-based formulation was developed to analyze two-dimensional thermal-structural problems. The flux-based formulation was developed and applied to the nodeless variable finite element in order to reduce the computational complexity as compared to the conventional finite element method. An adaptive meshing technique was implemented to further improve the solution accuracy. The performance of the combined procedure was evaluated by using two problems. These problems demonstrate that the combined nodeless variable finite element method using the flux-based formulation with the adaptive meshing technique helps increasing the solution accuracy while reducing the unknowns as compared to the conventional method.

References

[1] Phongthanapanich S and Dechaumphai P 2006 *Adv. Eng. Software* **27** 797-804
[2] Cheng Z and Paraschivoiu M 2003 *Finite Elem. Anal. Des.* **39(7)** 581-97
[3] Eibner T and Melenk J M 2007 *Comput. Mech.* **39(5)** 575-95
[4] Phongthanapanich S and Dechaumphai P 2004 *Trans. of the CSME* **27** 319-39
[5] Phongthanapanich S and Dechaumphai P 2004 *Trans. of the CSME* **28** 531-50
[6] Phongthanapanich S, Traivivatana S, Boonmaruth P and Dechaumphai P 2006 *Acta Mech. Sinica* **22(2)** 138-47
[7] Babuska I, Banerjee U and Osborn J E 2007 *Numer. Math.* **107(3)** 353–95
[8] Zienkiewicz O C and Zhu J Z 1992 *Int. J. Numer. Methods Engrg*. **33** 1365-82
[9] Becker R, Hansbo P and Larson M G 2003 *Comput. Meth. Appl. Mech. Eng.* **192(5-6)** 723-33
[10] Huang C-S, Leeb C-F and Cheng A H-D 2007 *Eng. Anal. Bound. Elem.* **31(7)** 614-23
[11] Lesaint P and Zlamal M 1979 *RAIRO Anal. Numer.* **13** 139-66